


Clinical mutations in the *TERT* and *TERC* genes coding for telomerase components induced oxidative stress, DNA damage at telomeres and cell apoptosis besides decreased telomerase activity

Beatriz Fernández-Varas¹, Cristina Manguan-García^{1,2}, Javier Rodríguez-Centeno¹, Lucía Mendoza-Lupiañez¹, Joaquín Calatayud³, Rosario Perona^{2,4}, Mercedes Martín-Martínez⁵, Marta Gutierrez-Rodríguez⁵, Carlos Benítez-Buelga^{1,*}, Leandro Sastre ^{1,2,*}

¹Instituto de Investigaciones Biomédicas Sols/Morreale CSIC/UAM, Arturo Duperier 4, 28029 Madrid, Spain

²Centro de Investigación Biomedica en Red de Enfermedades Raras (CIBERER), Instituto de Salud Carlos III. C. Melchor Fernandez de Almagro, 3, 28029 Madrid, Spain

³Departamento de Biología y Geología, Física y Química inorgánica. ESCET, Universidad Rey Juan Carlos, C/Tulipán s/n, Móstoles, C.P. 28933 Madrid, Spain

⁴Instituto de Salud Carlos III. Calle Monforte de Lemos 5, 28029 Madrid, Spain

⁵Instituto de Química Médica CSIC, Juan de la Cierva 3, 28006 Madrid, Spain

*Corresponding authors: Instituto de Investigaciones Biomédicas Sols/Morreale CSIC/UAM. Arturo Duperier 4, 28029 Madrid, Spain. E-mail lsastre@iib.uam.es and cbbuelga@iib.uam.es

Abstract

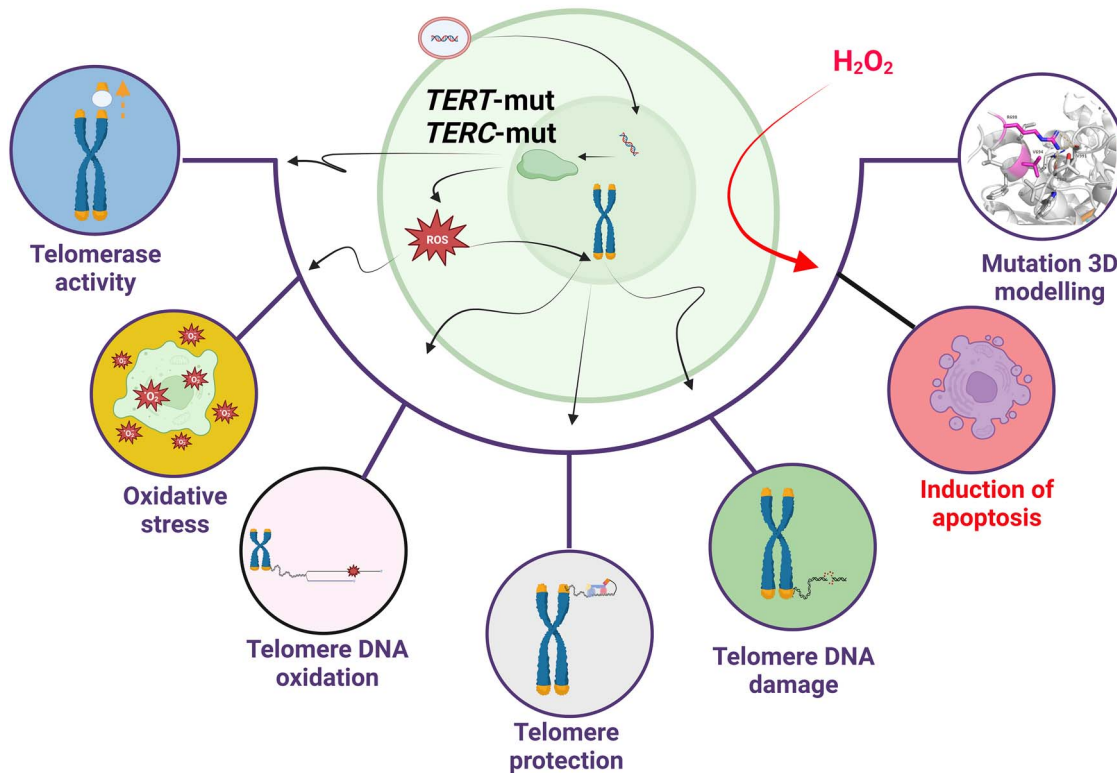
Telomeres are nucleoprotein structures at the end of chromosomes that maintain their integrity. Mutations in genes coding for proteins involved in telomere protection and elongation produce diseases such as dyskeratosis congenita or idiopathic pulmonary fibrosis known as telomeropathies. These diseases are characterized by premature telomere shortening, increased DNA damage and oxidative stress. Genetic diagnosis of telomeropathy patients has identified mutations in the genes *TERT* and *TERC* coding for telomerase components but the functional consequences of many of these mutations still have to be experimentally demonstrated. The activity of twelve *TERT* and five *TERC* mutants, five of them identified in Spanish patients, has been analyzed. *TERT* and *TERC* mutants were expressed in VA-13 human cells that express low telomerase levels and the activity induced was analyzed. The production of reactive oxygen species, DNA oxidation and TRF2 association at telomeres, DNA damage response and cell apoptosis were determined. Most mutations presented decreased telomerase activity, as compared to wild-type *TERT* and *TERC*. In addition, the expression of several *TERT* and *TERC* mutants induced oxidative stress, DNA oxidation, DNA damage, decreased recruitment of the shelterin component TRF2 to telomeres and increased apoptosis. These observations might indicate that the increase in DNA damage and oxidative stress observed in cells from telomeropathy patients is dependent on their *TERT* or *TERC* mutations. Therefore, analysis of the effect of *TERT* and *TERC* mutations of unknown function on DNA damage and oxidative stress could be of great utility to determine the possible pathogenicity of these variants.

Received: October 2, 2023. Revised: January 16, 2024. Accepted: January 17, 2024.

© The Author(s) 2024. Published by Oxford University Press. All rights reserved. For Permissions, please email: journals.permissions@oup.com

This is an Open Access article distributed under the terms of the Creative Commons Attribution Non-Commercial License (<https://creativecommons.org/licenses/by-nc/4.0/>), which permits non-commercial re-use, distribution, and reproduction in any medium, provided the original work is properly cited. For commercial re-use, please contact journals.permissions@oup.com

Graphical Abstract

Cloning, transfection and characterization of patient *TERT* and *TERC* mutations

Keywords: TERT/TERC; DNA damage; oxidative stress; apoptosis; telomeropathies

Introduction

Reduced size of telomeres, the structures that protect chromosome ends [1], is at the origin of several human diseases named telomeropathies, telomere biology diseases (TBDs) or short-telomere syndromes [2, 3]. Among these rare diseases are dyskeratosis congenita (DC, OMIM numbers 613989, 127550), idiopathic pulmonary fibrosis (IPF, OMIM numbers 614742, 614743) and some cases of aplastic anemia (AA, OMIM 614742, 614743) [2]. Telomere replication is not complete at the 3' end of the DNA and their size decreases with age in somatic cells which is one of the causes of organism aging [4, 5]. In TBD patients telomere shortening is more pronounced and manifests at an early age due to mutations in genes coding for proteins involved in telomere extension and protection [6]. These two functions are achieved by the telomerase and shelterin complexes, respectively.

DC, AA and IPF human diseases have been linked to variants within the genes that encode for the two telomerase essential core components, telomerase RNA (TR, encoded by the *TERC* gene) and telomerase reverse transcriptase (*TERT*); as well as in other genes encoding for telomerase-associated proteins of the H/ACA complex (*DKC1*, *NOP10*, *NHP2* and *GAR1*) [7]. Heterogeneous mutations in these genes have shown to impact telomerase function at different degree and are associated with short telomere length as well as with genetic anticipation in affected TBD patients [8].

The structure of the human telomerase holoenzyme has been determined by cryo-electron microscopy [9, 10] showing the existence of two RNA-tethered lobes. One of the lobes is composed

by a TERT monomer bound to the 5' terminal region of the TR RNA. The other lobe contains the 3' part of TR bound to a dimer of the associated H/ACA proteins. The TR domains that interact with TERT include the template/pseudoknot domain (t/PK) that contains the template region used for telomere elongation and the conserved regions 4 and 5 (CR4/5) [11]. Interaction with *DKC1* and associated proteins takes place through the ScRNA domain [12]. The TERT protein is composed of four domains: essential N-terminal domain (TEN), high-affinity RNA-binding domain (TRBD), reverse transcriptase domain (RT) and C-terminal extension (CTE) [11]. The protein has a ring structure and contacts are established at one side through the TRBD and CTE of TERT and the CR4-CR5 TR domain, and through the t/PK domain of TR and the catalytic center of the enzyme at the other side. Recruitment of the TERT holoenzyme to telomeres requires binding to some proteins of the shelterin complex such as *POT1* and *TPP1* [13, 14]. Interactions with these proteins also regulate telomerase activity and processivity [15, 16].

Besides its prominent role in telomere extension, TERT has been also involved in other cellular processes. For example, TERT interacts with transcription factors to regulate gene expression [17–19]. In addition, TERT has been found bound to mitochondria and is proposed to regulate cell apoptosis through this interaction [20–22].

Current genetic analysis has shown that TBD patients can carry mutations in 15 different genes, including *TERT* and *TERC* as some of the more frequently affected [7, 23, 24]. These variants result in

telomere shortening and, when a number of telomeres reach a critical minimal size, they are recognized as damaged DNA and a signaling pathway is activated that can result in cellular senescence or apoptosis [25, 26]. This process affects tissue stem cells and produces impaired tissue renewal and premature aging [25, 27, 28]. Animal models and cell lines obtained from patients have also shown an increase in oxidative stress that can contribute to induce cell apoptosis [29, 30].

Classically, functional characterization of patient's variants is made by expressing *TERT* or *TERC* mutations in a telomerase deficient cell line to evaluate *in vitro* telomerase activity in the cellular extracts of transfected cells [31–33]. In this way, it is possible to propose that variants with decreased telomerase activity are responsible for the presence of short telomeres in patients. However, besides the role of telomerase in the maintenance of telomere length avoiding the DNA damage response, *TERT* has been implicated in the response to oxidative stress, as mentioned above. In this context *TERT* increases its localization to the mitochondria protecting cells from apoptosis and DNA damage [21, 34]. Hence, a complete characterization of *TERT* and *TERC* variants would require the evaluation of both the effect on telomerase activity as well as on oxidative stress and DNA damage responses.

In this study functional activity of 4 *TERT* and 1 *TERC* variants found in a Spanish cohort of TBD patients was analyzed for the above-mentioned parameters. In addition, this study was extended to 8 *TERT* and 4 *TERC* additional variants that were previously characterized in terms of *in vitro* telomerase activity. Using targeted mutagenesis, these 12 *TERT* and 5 *TERC* mutations found in patients with DKC, IPF or AA were generated. These variants were transiently transfected into VA-13 human cells, which are non-cancerous lung fibroblasts that express *TERT* in minimal levels. Next, the impact of the mutations on the telomerase activity as well as other phenotypes associated with oxidative stress, DNA damage and apoptosis were evaluated. The results obtained indicate that several *TERT* and *TERC* variants showed decreased telomerase activity and also induced oxidative stress, DNA damage response, altered telomere localization of the shelterin-complex component TRF2 or increased apoptosis. Actually, some mutations alter these cellular activities even if they show telomerase activity similar to wild type *TERT* supporting the convenience of more extensive functional studies of *TERT* and *TERC* variants, besides *in vitro* telomerase activity.

Results

Determination of the telomerase activity of *TERT* and *TERC* mutants

Twelve *TERT* and five *TERC* mutations described in TBD patients (information summarized in Table 1) were independently generated on the pBABE-*TERT/TERC* vector by site-directed mutagenesis. This vector directs the expression of both the *TERT* protein and the TR RNA allowing the assembly of the active telomerase enzyme in transfected cells. To determine the telomerase activity of the enzymes carrying *TERT* and *TERC* mutations, the cell line VA-13, with low levels of telomerase activity was used for transfection. The expression levels of *TERT* and *TERC* in transfected cells were determined by RT-q-PCR (Supplementary Fig. S1). Cellular extracts were prepared from VA-13 cells 24 h after transfection with the pBABE-*TERT/TERC* vectors that expressed the different variants of the genes, the vector expressing the wild-type genes and the pBABE empty vector to measure telomerase activity using the TRAP assay. A significant increment of telomerase activity in the pBABE-WT *TERT/TERC* transfected cells compared

to those transfected with the pBABE empty vector was observed (Fig. 1). On the other hand, VA-13 cells expressing *TERT* (Fig. 1A) and *TERC* (Fig. 1B) mutants presented a significant reduction of telomerase activity when compared to the pBABE-WT *TERT/TERC* transfected cells in most cases. However, no significant effect was found for four *TERT* mutants, 2/5 within the TEN domain (p.Pro65Thr, p.Ala202Thr), 1/5 within the RT domain (p.Tyr772Cys) and 1/2 within the CTE domain (p.Thr1101Met). Similarly, 1/2 *TERC* mutants within the CR4/5 domain (n.325G > T) showed telomerase activity similar to the wild-type gene. Representative TRAP assays are shown in Supplementary Fig. S2.

Effect of *TERT/TERC* mutations on the production of reactive oxygen species (ROS)

Besides its role in telomere elongation, *TERT* has been related to the regulation of cellular oxidative stress (OS) through mitochondrial interaction. The effect of *TERT/TERC* mutations in the production of ROS was studied using DHE as probe to detect O₂⁻. Both nuclear (Fig. 2), and cytoplasmic ROS signals (Supplementary Fig. S3) were determined and quantified. The results obtained for nuclear ROS (Fig. 2) indicated that expression of WT *TERT* and *TERC* slightly decreases ROS production, although the difference is not statistically significant. On the contrary, significantly increased ROS levels were observed for cells expressing six *TERT* mutants (Fig. 2B) and four *TERC* mutants (Fig. 2C). Out of the *TERT* variants that increased oxidative stress, p.Val84Glu, p.Phe159CysfsTer32 and p.Ala202Thr are located in the TEN domain, p.Arg698Thr and p.Val747AlafsTer20 in the RT domain and p.Thr1101Met in the CTE domain. Variants p.Arg865Cys and p.Val1090Met also induced higher DHE intensity than the control but the difference was not statistically significant. In the case of *TERC*, there were variants involved in the three structural domains considered and only n.269G > A did not induce significantly increased DHE staining. The results obtained for cytoplasmic ROS (Supplementary Fig. S3) are in general agreement with those of nuclear ROS. Among the few differences are variant p.Phe159CysfsTer32, that showed a tendency to increase cytoplasmic ROS levels (P: 0.05), p.Arg698Thr and p.Val747AlafsTer20 that did not show significant changes in cytoplasmic ROS levels. *TERC* variants also produce similar variations in nuclear and cytoplasmic ROS levels although the increase produced by n.98G > A was significant in nuclear ROS and not in the cytoplasmic one and the reverse results were obtained for n.269G > A. These results suggest that some *TERT/TERC* mutants induce the formation of ROS.

Effect of *TERT/TERC* mutations on oxidative DNA damage accumulation at telomere DNA

Increased cellular ROS induces guanine oxidation on the DNA, which results in DNA damage and genome instability. Therefore, the possible accumulation of oxidative DNA damage induced by the expression of *TERT* or *TERC* mutations was determined at telomeres. We measured the relative amount of oxidized lesions by a qPCR-based method [35].

The results obtained indicated that expression of wild-type *TERT* and *TERC* decreased oxidative DNA damage at telomeres (Fig. 3). In these experiments non-transfected VA-13 cells were incubated with 20 mM KBrO₃ for 1 h to induce oxidative stress, as a positive control. When comparing oxidative DNA damage in cells transfected with *TERT/TERC* mutants with those transfected with WT genes, we found that nine *TERT* mutations (Fig. 3A) and four *TERC* mutations (Fig. 3B) increased oxidative DNA damage at telomeres. Only one mutant at the *TERT* TEN domain

Table 1. Description of the nucleotide variants analyzed.

| Gene. | Nucleotide variant | Amino acid variant | Associated disease | Variant reference | Bibliographic Reference |
|--------------|--------------------|------------------------|--------------------|-------------------|-------------------------|
| TERT | c.164T>A | p.Leu55Gln | IPF | rs387907247 | [59] |
| | c.193C>A | p.Pro65Thr | AA, AML | rs544215765 | [41] |
| | c.251T>A | p.Val84Glu | AA | none assigned | [41] |
| | c.475_76delTT | p.Phe159Cys fsTer32 | DC | none assigned | [41] |
| | c.604G>A | p.Ala202Thr | AA | rs121918661 | [55] |
| | c.2080G>A | p.Val694Met | AA, IPF, cancer | rs121918662 | [32] |
| | c.2092C>T | p.Arg698Trp | DC | rs866282352 | [53] |
| | c.2240delT | p.Val747Ala fsTer20 | IPF | rs199422300 | [45] |
| | c.2315A>G | p.Tyr772Cys | AA | rs121918663 | [32] |
| | c.2593C>T | p.Arg865Cys | IPF | rs372868296 | [45] |
| | c.3268G>A | p.Val1090Met | AA | rs121918664 | [32] |
| | c.3302C>T | p.Thr1101Met | DC | rs764602705 | This article |
| | TERC | n.23G>C | | IPF | none assigned |
| n.96_97delCT | | | DC,IPF,AA | rs199422267 | [8] |
| n.98G>A | | | IPF | rs199422268 | [59] |
| n.269G>A | | | IPF | none assigned | [41] |
| n.325G>T | | | IPF | none assigned | [54] |

TERT: NM_001193376.1; TERC: NR_001566.1. AA: aplastic anemia; AML: acute myeloblastic leukemia; DC: dyskeratosis congenita; IPF: idiopathic pulmonary fibrosis.

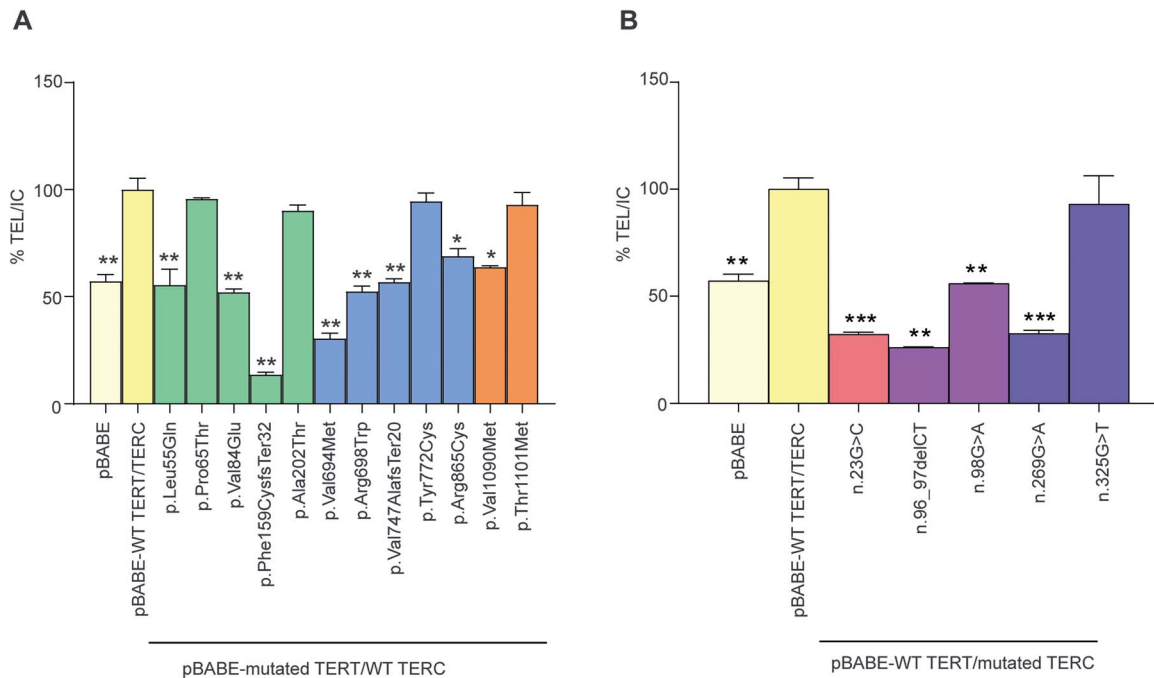


Figure 1. Telomerase activity in TERT/TERC mutants. Telomerase activity was measured by TRAP assay in VA-13 cells transfected with pBABE empty vector (transfection control), pBABE-WT TERT/TERC (WT telomerase) or the different TERT (panel A) and TERC mutants (panel B). Telomerase activity was quantified and normalized to an internal control (IC) and expressed as a percentage relative to pBABE-WT TERT/TERC (considered as 100%). The colors of the bars represent the different gene domains in which the mutations are found: yellow (controls: pBABE and pBABE WT TERT/TERC), light green (TEN: p.Leu55Gln to p.Ala202Thr), light blue (RT: p.Val694Met to p.Arg865Cys), orange (CTE: p.Val1090Met and p.Thr1101Met) for TERT and pink (P1a stem: n.23G>C), purple (t/PK: n.96_97delCT and n.98G>A), dark blue (CR4/5: n.269G>A and n.325G>T) for TERC. The experiments were repeated two times with similar results and mean values \pm SEM of the triplicates of a representative experiment are shown. Statistical significance between pBABE-WT TERT/TERC and each TERT or TERC mutant was calculated using two-tailed unpaired t-test (* $P < 0.05$; ** $P < 0.01$; *** $P < 0.001$). The images of the assay are shown in [Supplementary Fig. S2](#).

(p.Pro65Thr) and one within the CTE domain (p.Thr1101Met) did not present significant increased levels of oxidized DNA damage at telomeres. The TEN-domain mutant p.Leu55Gln produced lower oxidative damage than the control vector expressing WT

TERT and TERC. Also, four of the five TERC mutants presented significant accumulation of oxidized lesions at telomeres and only the variant n.98G>A did not induce increased DNA damage at telomeres.

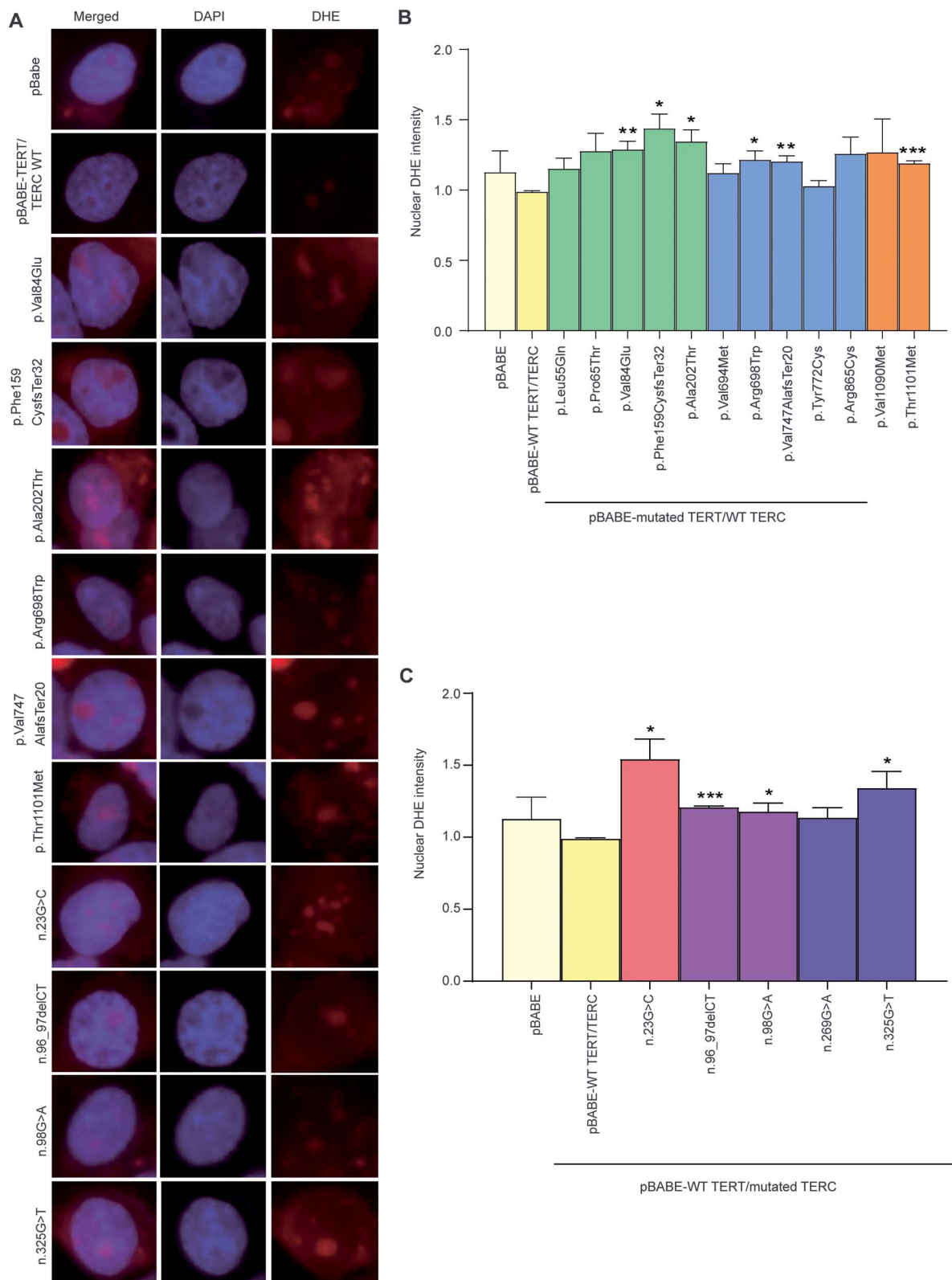


Figure 2. Reactive oxygen species (ROS) levels in *TERT/TERC* mutants. ROS were detected with the DHE probe in VA-13 cells transfected with pBABE empty vector (transfection control), pBABE-WT *TERT/TERC* (WT telomerase) or the different *TERT* and *TERC* mutants. (A) Representative wide-field microscopy images of single cells are shown for those mutants that presented significant differences compared to pBABE-WT *TERT/TERC*. In blue, counterstaining of nuclei with DAPI. In red, the DHE probe for ROS detection. (B, C) Nuclear DHE intensity was quantified for *TERT* (B) and *TERC* (C) mutants and normalized to pBABE-WT *TERT/TERC*. The colors of the bars represent the different gene domains in which the mutations are found: yellow controls: pBABE and pBABE-WT *TERT/TERC*, light green (TEN: p.Leu55Gln to p.Ala202Thr), light blue (RT: p.Val694Met to p.Arg865Cys), orange (CTE: p.Val1090Met and p.Thr1101Met) for *TERT* and pink (P1a stem: n.23G>C), purple (t/PK: n.96_97delCT and n.98G>A), dark blue (CR4/5: n.269G>A and n.325G>T) for *TERC*. Graph bars represent mean values \pm SEM of three independent experiments. The value of each experiment is the mean nuclear DHE intensity of five different microscopy fields (average of 200 cells/experiment). Statistical significance between pBABE-WT *TERT/TERC* and each *TERT* or *TERC* mutant was calculated using two tailed unpaired t-test (* $P < 0.05$; ** $P < 0.01$; *** $P < 0.001$).

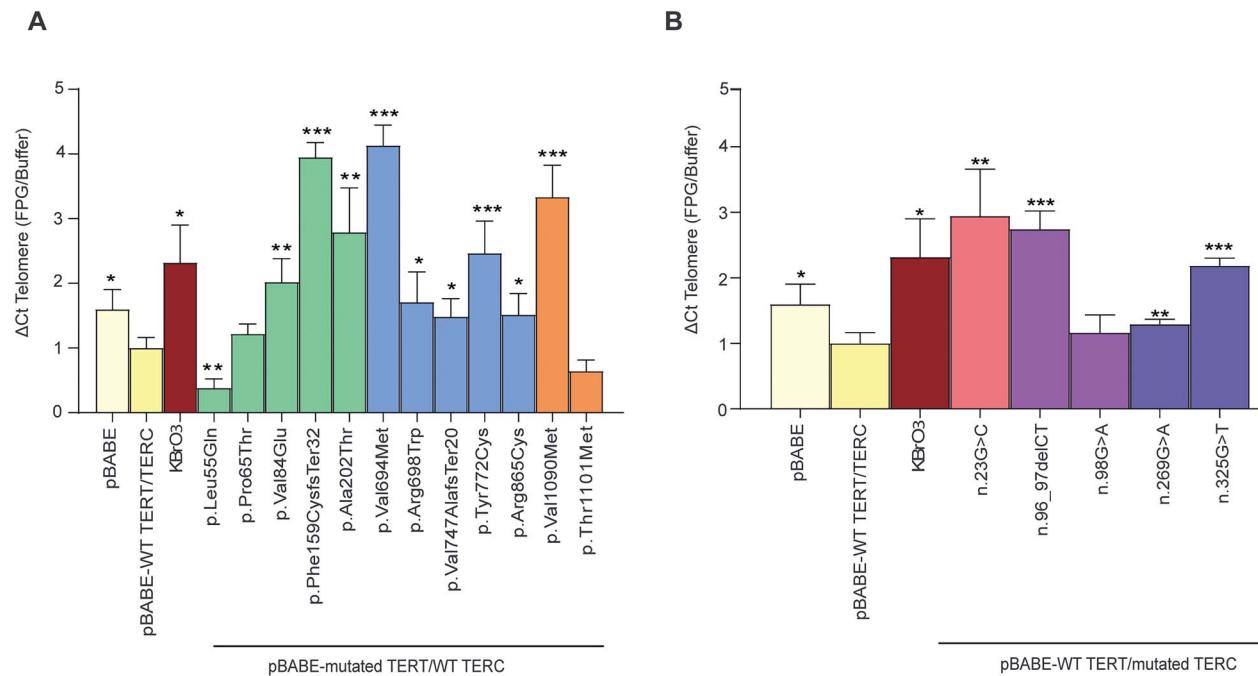


Figure 3. Oxidative DNA damage at telomeres in *TERT/TERC* mutants. Oxidative DNA damage at telomeres was analyzed by qPCR in VA-13 cells transfected with pBABE empty vector (transfection control), pBABE-WT *TERT/TERC* (WT telomerase) or the different *TERT* (panel A) and *TERC* (panel B) mutants. Potassium bromate (KBrO₃) was used as a positive control. The differences in PCR kinetics (Ct) between FPG-digested vs undigested DNA are represented for each sample as Δ Ct Telomere (FPG/Buffer) and normalized to pBABE-WT *TERT/TERC*. Colors of the bars represent the different gene domains in which the mutations are found: yellow (controls: pBABE and pBABE-WT *TERT/TERC*), light green (TEN: p.Leu55Gln to p.Ala202Thr), light blue (RT: p.Val694Met to p.Arg865Cys), orange (CTE: p.Val1090Met and p.Thr1101Met) for *TERT* and pink (P1a stem: n.23G>C), purple (t/PK: n.96_97delCT and n.98G>A), dark blue (CR4/5: n.269G>A and n.325G>T) for *TERC*. Graph bars represent mean values \pm SEM of eight technical replicates from two independent experiments. Statistical significance between pBABE-WT *TERT/TERC* and each *TERT* or *TERC* mutant was calculated using two-tailed unpaired t-test (* $P < 0.05$; ** $P < 0.01$; *** $P < 0.001$).

Effect of *TERT/TERC* mutations on TRF2 recruitment to telomeres

Telomerase mutations could alter recruitment of telomerase to telomeres and also the interaction with the shelterin complex. Both telomere recruitment and shelterin interaction regulate telomerase activity independently of the basal enzymatic activity determined *in vitro*, as shown in Fig. 1. In addition, oxidative DNA damage has been previously identified to interfere with TRF2-telomere binding [36] as well as being a determinant in telomerase recruitment [37] to the telomere. Therefore, the ability of *TERT/TERC* mutants to recruit the TRF2 shelterin component to the telomere was tested by FISH-immunolocalization. Telomeres were identified by FISH using a telomere-specific fluorescent probe (TelC) and TRF2 by immunofluorescence using a specific antibody.

Recruitment of TRF2 to telomeres increased when the WT *TERT* and *TERC* genes were expressed and decreased upon oxidative stress induced by 2 mM KBrO₃ incubation overnight (Fig. 4). TRF2-telomere overlapping was significantly reduced by two *TERT* mutants at the TEN domain, p.Val84Glu and p.Ala202Thr (Fig. 4B). Two *TERC* mutants, n.96_97delCT, placed at t/PK and n.325G>T, at the CR4/5 domains also decreased TRF2 recruitment to telomeres (Fig. 4C).

Effect of *TERT/TERC* mutations on the DNA damage response at telomeres

Telomere uncapping can trigger the DNA damage response (DDR) [38]. Previous experiments have shown that *TERT* and *TERC* mutants can impair TRF2 binding to telomeres (Fig. 4) and

increase oxidative damage (Fig. 3). Because of these observations, the possible presence of a DNA damage response at telomeres was analyzed. In these experiments DNA damage response was identified by binding of the 53BP1 protein to the DNA using one specific antibody. The overlapping index between 53BP1 and the TelC probe (TIF-53BP1) was determined to evaluate telomeric DNA damage in response to the expression of *TERT/TERC* mutants. In addition, we calculated the number of nuclear foci on transfected cells to test whether induction of DNA damage was specific of telomeres or more general.

Co-localization of 53BP1 at telomeres decreased upon expression of wild-type *TERT/TERC* and increased by overnight treatment of these cells with 2 mM KBrO₃, as shown in Fig. 5. Expression of several *TERT* and *TERC* variants increased DDR at telomeres with significant differences observed in the case of six *TERT* (p.Leu55Gln, p.Pro65Thr, p.Val84Glu, p.Val202Thr, p.Arg698Trp and p.Val1090Met, Fig. 5B) and four *TERC* (n.23G>C, n.96_97delCT, n.98G>A and n.269G>A, Fig. 5C) mutants. On the contrary, in one mutant at the TEN domain, four at the RT and one at the CTE domain of *TERT* and the n.325G>T mutant of *TERC* the increase of 53BP1 association to telomeres was not statistically significant although the *TERT* mutant p.Arg865Cys and the *TERC* mutant n.325G>T showed a tendency to increased damage.

The number of nuclear 53BP1 foci also decreased upon wild-type *TERT/TERC* expression and increased when oxidative stress was induced by KBrO₃ treatment (Fig. 6). The expression of two *TERT* (p.Val84Glu and p.Arg698Trp) and one *TERC* (n.98G>A) mutants increased significantly the number of nuclear 53BP1 loci. Additionally, six other *TERT* (p.Pro65Thr, p.Ala202Thr, p.Val694Met, p.Tyr772Cys, p.Arg865Cys and p.Val1090Met) and

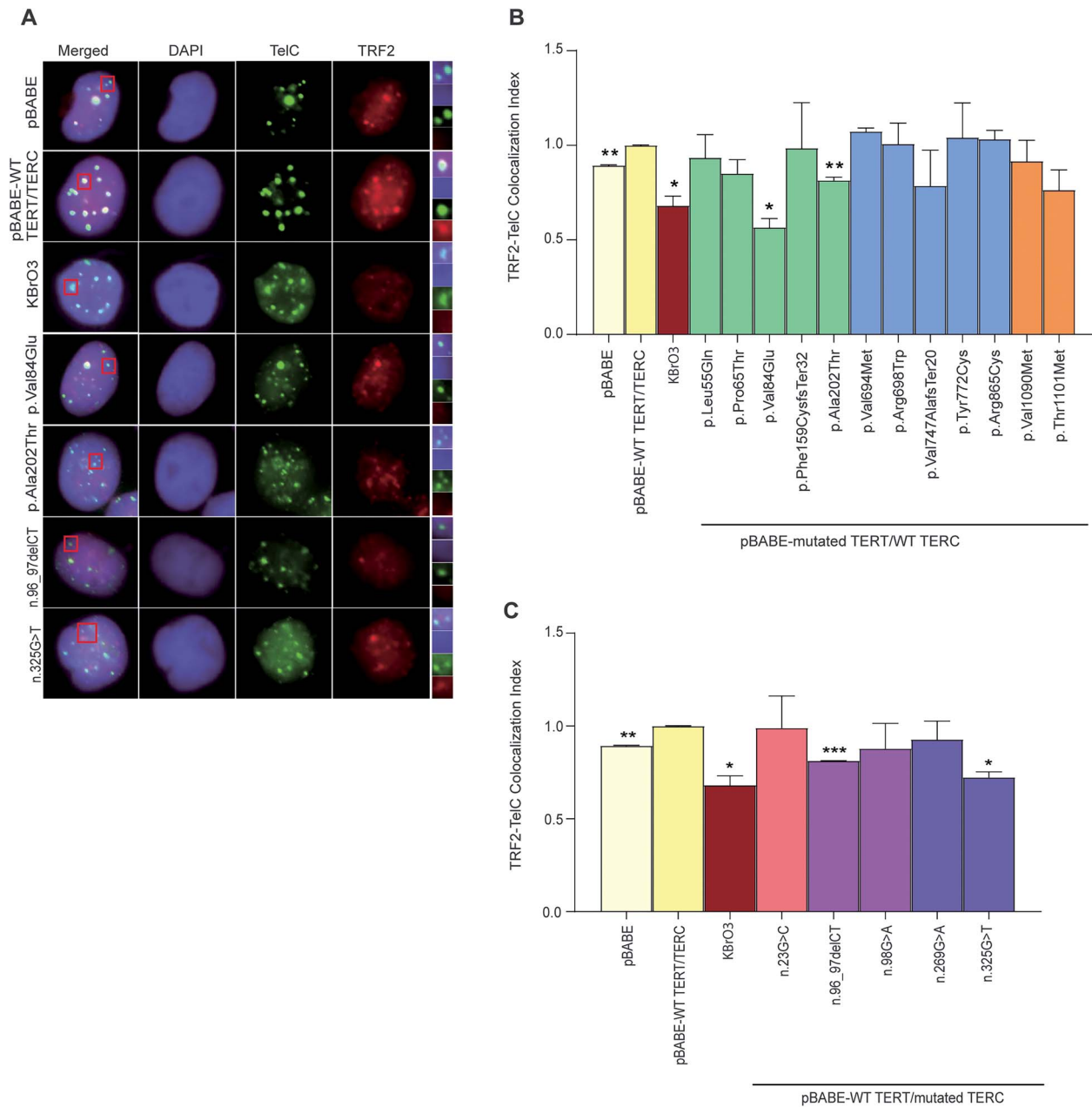


Figure 4. Telomere protection in *TERT/TERC* mutants. Telomere protection was determined by measuring colocalization of TRF2 protein and PNA-TelC telomeric probe in VA-13 cells transfected with pBABE empty vector (transfection control), pBABE-WT *TERT/TERC* (WT telomerase) or with the different *TERT* (panel A, B) and *TERC* (panels A, C) mutants. Potassium bromate (KBrO_3) was used as a positive control. (A) Representative wide-field microscopy images of single cells are shown for those mutants that presented significant differences compared to pBABE-WT *TERT/TERC*. The red square is magnified in a panel at the right side of the image, to point at telomeres that overlap with TRF2. In blue, counterstaining of nuclei with DAPI. In green, the PNA-TelC probe hybridizing with telomere DNA. In red, TRF2 shelterin protein. (B, C) TRF2-TelC overlapping index was quantified and normalized to pBABE-WT *TERT/TERC*. The colors of the bars represent the different gene domains in which the mutations are found: yellow (controls: pBABE and pBABE-WT *TERT/TERC*), light green (TEN: p.Leu55Gln to p.Ala202Thr), light blue (RT: p.Val694Met to p.Arg865Cys), orange (CTE: p.Val1090Met and p.Thr1101Met) for *TERT* and pink (P1a stem: n.23G>C), purple (t/PK: n.96_97delCT and n.98G>A), dark blue (CR4/5: n.269G>A and n.325G>T) for *TERC*. Graph bars represent mean values \pm SEM of two independent experiments. The value of each experiment is the mean TRF2-TelC overlapping index of five different microscopy fields (average of 200 cells/experiment). Statistical significance between pBABE-WT *TERT/TERC* and each *TERT* (B) or *TERC* mutant (C) was calculated using two tailed unpaired t-test (* $P < 0.05$; ** $P < 0.01$; *** $P < 0.001$).

three *TERC* (n.23G>C, n.96_97delCT and n.325G>T) mutants showed a tendency to increased DDR but the difference was not statistically significant. All mutants that increased nuclear DDR also increased 53BP1 localization at telomeres, although in the case of the *TERT* p.Ala202Thr mutant the difference was not statistically significant (Fig. 6A). The *TERC* mutants n.23G>C, n.96_97delCT, n.98G>A and n.325G>T showed increased levels

of 53BP1 telomere association and nuclear foci although in the last test the difference was only significant for n.98G>A (Fig. 6B). DNA damage at the cellular nuclei was also tested by the expression of the γ H2AX histone. The results indicated that wild-type *TERT/TERC* expression significantly decreased γ H2AX expression. Several mutants induced increased DNA damage response, in general agreement with the data obtained for 53BP1

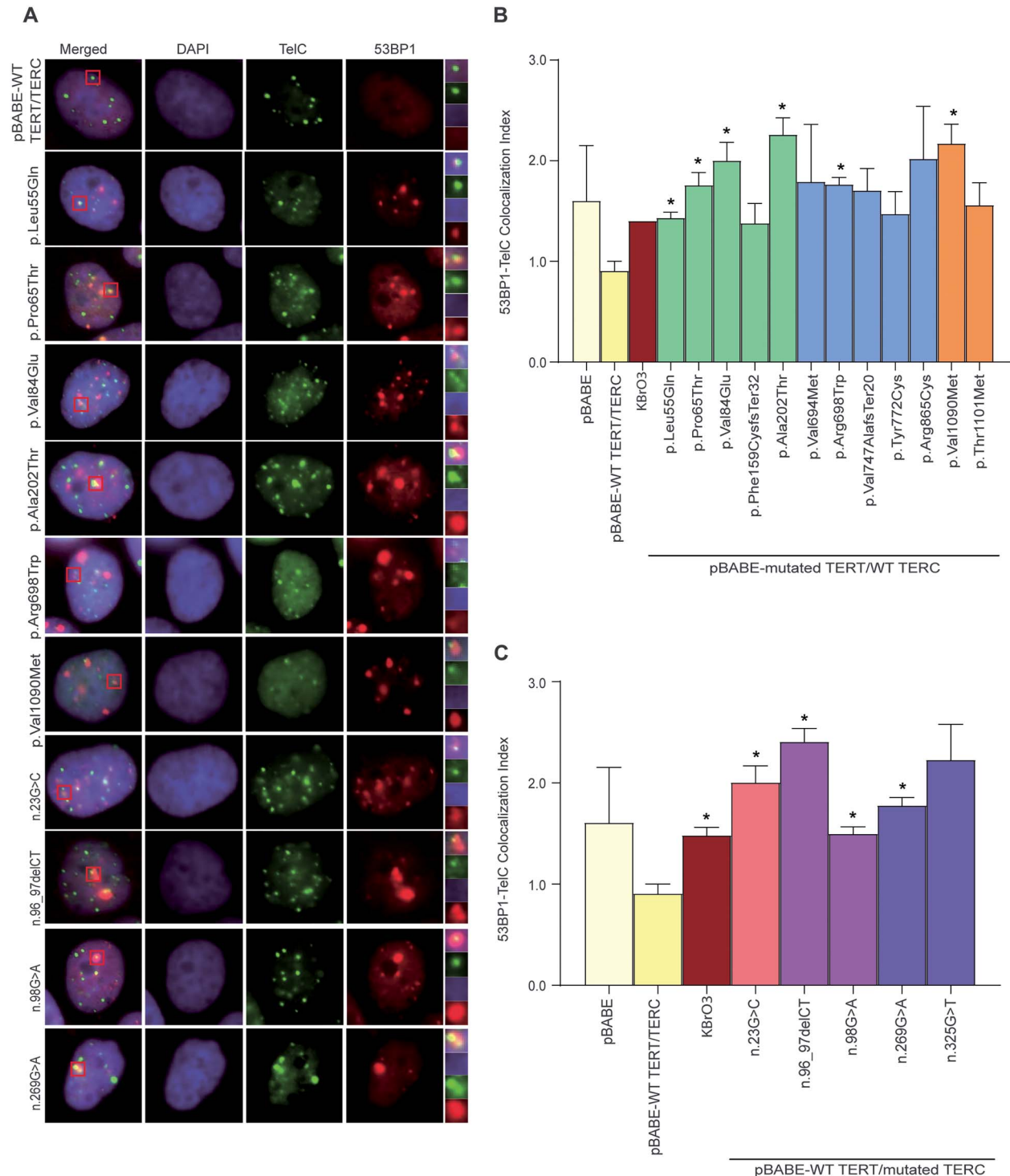


Figure 5. Activation of DNA damage response at telomeres in TERT/TERC mutants. Activation of DNA damage response at telomeres was determined by measuring colocalization of 53BP1 protein and PNA-TelC telomeric probe in VA-13 cells transfected with pBABE empty vector (transfection control), pBABE-WT TERT/TERC (WT telomerase) or with the different TERT and TERC mutants. Potassium bromate (KBrO₃) was used as a positive control. (A) Representative wide-field microscopy images of single cells are shown for those mutants that presented significant differences compared to pBABE-WT TERT/TERC. The red square is magnified in a panel at the right side of the image, to point at telomeres that overlap with 53BP1 (TIF). In blue, counterstaining of nuclei with DAPI. In green, PNA-TelC probe hybridizing with telomere DNA. In red, 53BP1 is a DNA damage marker. (B, C) 53BP1-TelC overlapping index was quantified and normalized to pBABE-WT TERT/TERC for TERT (panel B) and TERC (panel C) mutants. Colors of the bars represent the different gene domains in which the mutations are found: Yellow (controls: pBABE and pBABE-WT TERT/TERC), light green (TEN: p.Leu55Gln to p.Ala202Thr), light blue (RT: p.Val694Met to p.Arg865Cys), orange (CTE: p.Val1090Met and p.Thr1101Met) for TERT and pink (P1a stem: n.23G>C), purple (t/PK: n.96_97delCT and n.98G>A), dark blue (CR4/5: n.269G>A and n.325G>T) for TERC. Graph bars represent mean values \pm SEM of two independent experiments. The value of each experiment is the mean 53BP1-TelC overlapping index of five different microscopy fields (average of 200 cells/experiment). Statistical significance between pBABE-WT TERT/TERC and each TERT or TERC mutant was calculated using a two-tailed unpaired t-test (** $P < 0.05$; *** $P < 0.01$; **** $P < 0.001$).

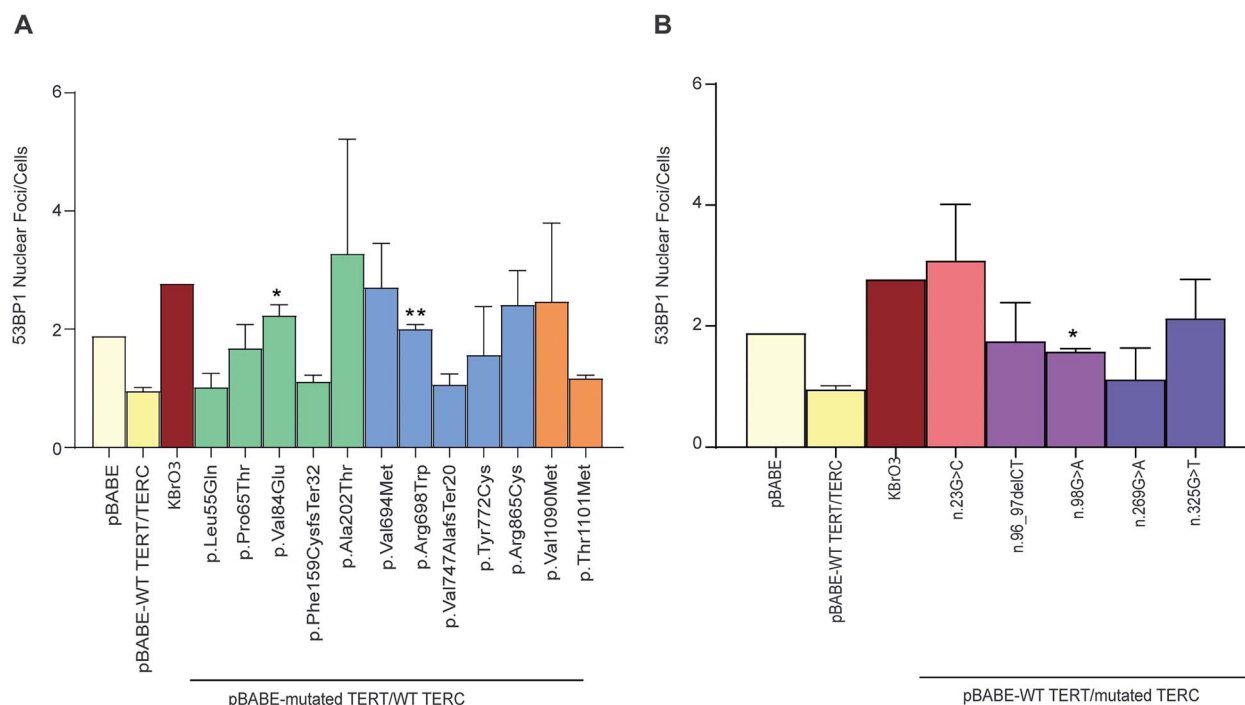


Figure 6. Activation of DNA damage response by *TERT/TERC* mutants. Activation of DNA damage response was determined by quantifying 53BP1 nuclear foci in VA-13 cells transfected with pBABE empty vector (transfection control), pBABE-WT *TERT/TERC* (WT telomerase) or with the different *TERT* (panel A) and *TERC* (panel B) mutants. Potassium bromate (KBrO₃) was used as a positive control. 53BP1 nuclear foci/cell were quantified and normalized to pBABE-WT *TERT/TERC*. The colors of the bars represent the different gene domains in which the mutations are found: yellow (controls: pBABE and pBABE-WT *TERT/TERC*), light green (TEN: p.Leu55Gln to p.Ala202Thr), light blue (RT: p.Val694Met to p.Arg865Cys), orange (CTE: p.Val1090Met and p.Thr1101Met) for *TERT* and pink (P1a stem: n.23G>C), purple (t/PK: n.96_97delCT and n.98G>A), dark blue (CR4/5: n.269G>A and n.325G>T) for *TERC*. Graph bars represent mean values ± SEM of two independent experiments. The value of each experiment is the mean 53BP1 nuclear foci/cell of five different microscopy fields (average of 200 cells/experiment). Statistical significance between pBABE-WT *TERT/TERC* and each *TERT* (A) or *TERC* mutant (B) was calculated using a two-tailed unpaired t-test (**P* < 0.05; ***P* < 0.01; ****P* < 0.001).

loci but the differences were statistically significant only for the p.Tyr772Cys mutant (Supplementary Fig. S4). These results would indicate that the DDR induced by *TERT* and *TERC* mutants is more important at telomeres than at the rest of the DNA.

Activity of *TERT/TERC* mutants on cell apoptosis induced by oxidative stress

TERT has been shown to translocate into the mitochondria and to regulate cell apoptosis. On the other hand, oxidative stress can induce cell apoptosis and previous results indicate that *TERT/TERC* mutants regulated ROS production (Fig. 2). Therefore, the possible effect of the expression of *TERT/TERC* mutants on cell apoptosis under basal conditions and induced by oxidative stress was analyzed. For that, *TERT/TERC* mutants were transfected into VA-13 cells and 16 h later exposed to a sub-lethal dose of H₂O₂ (1 mM) for a period of 3 h. Cells were allowed to recover by culture in fresh medium overnight. After this, cells were fixed and apoptosis measured determining Annexin V expression and propidium iodide (PI) incorporation by FACS cytometry. Late apoptosis was considered for cells expressing Annexin V and that incorporated PI (Fig. 7). Interestingly, transfection with pBABE-WT *TERT/TERC* showed a tendency to protect cells from late apoptosis although the data did not reach statistical significance. In contrast, cells expressing the TEN-domain mutants p.Val84Glu and p.Ala202Thr and the RT domain mutant p.Tyr772Cys showed a significant increase of late apoptosis under stress conditions (Fig. 7C). These mutants also showed a tendency to increase late apoptosis in basal conditions (Fig. 7A). Expression of the *TERC* mutant n.269G > A also induced an increase of cell apoptosis that

was statistically significant under oxidative stress (Fig. 7B and D). These data might indicate that specific *TERT* and *TERC* mutants might participate in oxidative stress response via apoptosis control.

The effects observed for *TERT* and *TERC* mutants have been summarized in Fig. 8 where mutants are schematically located on the corresponding domains of *TERT* or *TR* and the functional consequences of their expression on the biological activities assayed is indicated. In Supplementary Fig. S5 the different mutants have been grouped according to their activity by a hierarchical clustering. In this analysis only statistically significant differences have been considered. This analysis associates the mutants in two main groups, those that affect telomerase activity, oxidative stress and telomere DNA oxidation (seven *TERT* and three *TERC* mutants) and those that also affect late apoptosis and telomere TRF2 recruitment (three *TERT* and one *TERC* mutants). Three of the mutants do not decrease telomerase activity or induce apoptosis but increase oxidative stress (p.Thr1101Met, n.325G > T) or telomere DNA damage (p.Pro65Thr).

Mapping *TERT* variants to the three-dimensional (3D) structure of *TERT*

Twelve *TERT* mutations associated to diseases have been studied, ten of them involve the mutation of a sole residue. To enhance the understanding of the genetic variants, they were mapped into the cryo-EM structure of the complexes of human telomerase and telomeric DNA (PDB code 7BG9) [39], DNA-TPP1 (PDB code 7QXA) [40] and DNA-TPP1-POT1 (PDB codes 7QXB, 7QXS) [40]. This mapping has provided insights into the potential effects of the

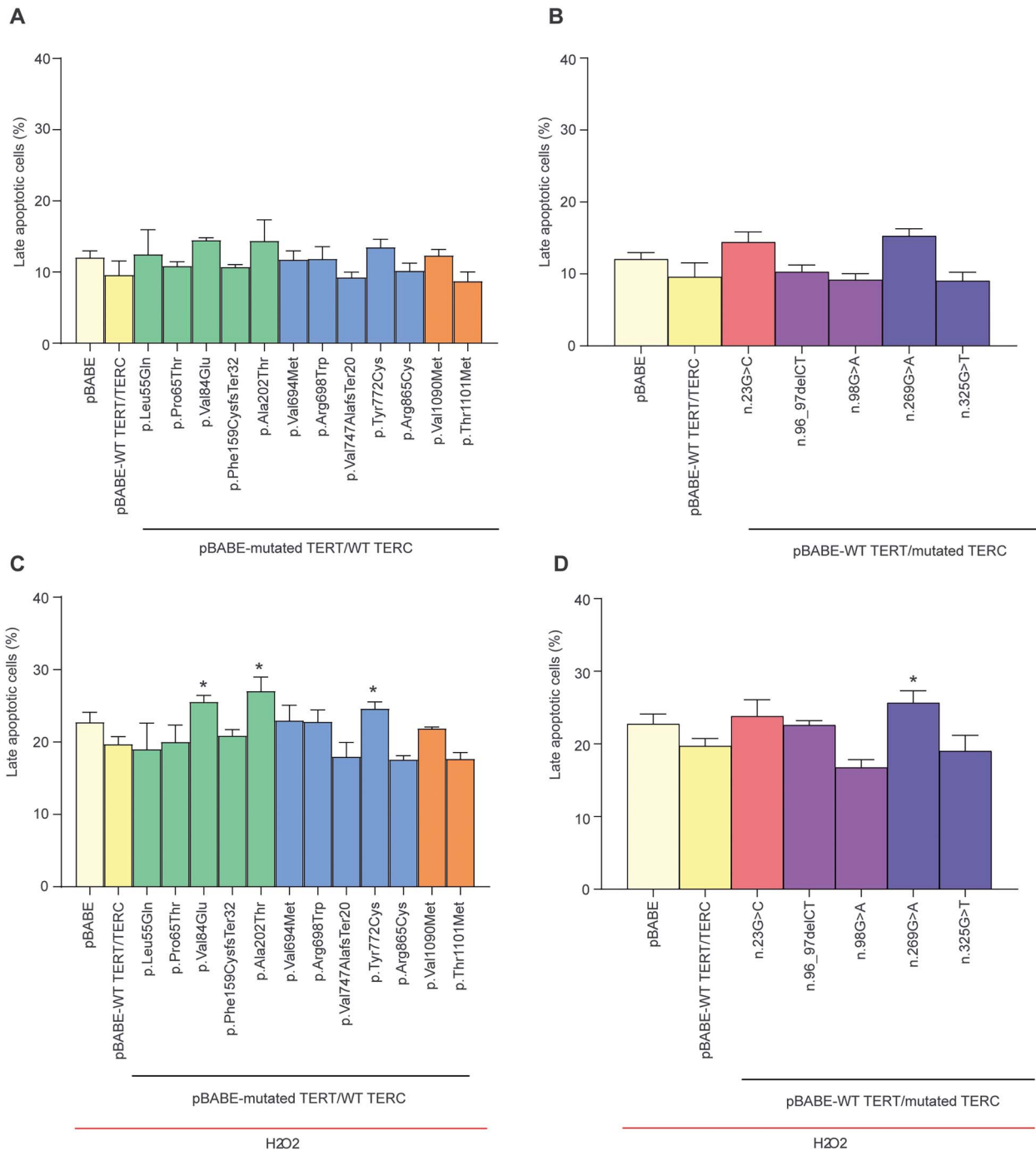


Figure 7. Induction of apoptosis in *TERT/TERC* mutants in basal conditions and under oxidative stress. Apoptosis was measured by determination of Annexin V expression and propidium iodide (PI) incorporation by FACS cytometry in VA-13 cells transfected with pBABA empty vector (transfection control), pBABA-WT *TERT/TERC* (WT telomerase) or the different *TERT* (panels A, C) and *TERC* (panels B, D) mutants. 16 h after transfection cells were exposed to a sublethal dose of H₂O₂ (1 mM) for 3 h in panels C and D. Cells were allowed to recover by culture in fresh media overnight. The total number of cells undergoing late apoptosis is represented. The colors of the bars represent the different gene domains in which the mutations are found: yellow (controls: pBABA and pBABA-WT *TERT/TERC*), light green (TEN: p.Leu55Gln to p.Ala202Thr), light blue (RT: p.Val694Met to p.Arg865Cys), orange (CTE: p.Val1090Met and p.Thr1101Met) for *TERT* and pink (P1a stem: n.23G>C), purple (t/PK: n.96_97delCT and n.98G>A), dark blue (CR4/5: n.269G>A and n.325G>T) for *TERC*. Graph bars represent mean values \pm SEM of three independent experiments. In each condition of the experiments, 10 000 cells were analyzed. Statistical significance between pBABA-WT *TERT/TERC* and each *TERT* or *TERC* mutant was calculated using a two-tailed unpaired t-test (**P* < 0.05; ***P* < 0.01; ****P* < 0.001).

mutation on protein stability, DNA-, RNA- and protein-protein interactions. Then, the possible alterations in the 3D structure surrounding each variant were compared with the functional consequences found in this study.

Three mutations are located in the reverse transcriptase domain of *TERT*, namely p.Val694Met, p.Arg698Trp and p.Arg865Cys. The structural analyses indicate that Val694 and Arg698 are in the same helix of the RT domain and establish

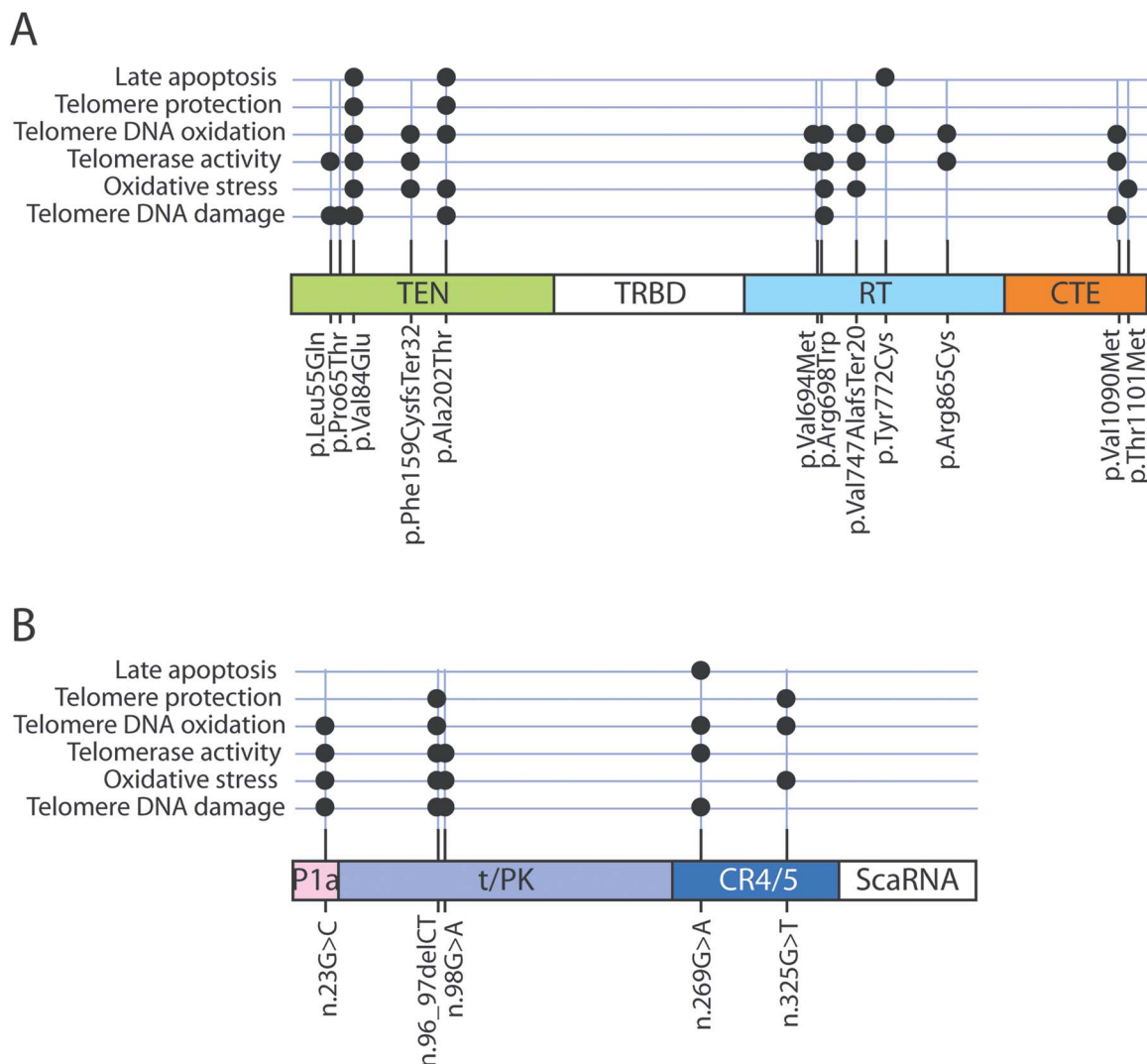


Figure 8. Schematic representation of the TERT and TERC variants analyzed and the results obtained. The variants analyzed in this article are located on the functional domains of the TERT protein (panel A) or the TR RNA (Panel B). Functional domains are labeled with the same colors used in Figs 1–7: light green (TEN), light blue (RT), orange (CTE) for TERT and pink (P1a stem), purple (t/PK) and dark blue (CR4/5) for TR. The domains where no variant was analyzed are indicated in white (TRBD domain for TERT and ScaRNA for TR). Significant differences observed in the functional assays performed, with respect to WT TERT/TERC are indicated as black circles for each variant above the diagrams.

contacts with adjacent residues, which could contribute to the stability of this domain (Fig. 9A). Their substitution by Met and Trp, respectively, could alter these interactions and disrupts protein packing. On the other hand, Arg865 is involved in a hydrogen bond network through its sidechain and Glu850 and Ser679 sidechains, as well as the Ser843 backbone CO. These interactions probably contribute to the adequate disposition of the catalytic center, including Asp712, Asp868 and Asp869 residues (Fig. 9B).

Leu55 is situated within a β sheet in the TEN domain, in proximity to the TR RNA, and to an α helix that directly interacts with the RNA (Fig. 10A). The substitution of this hydrophobic residue by a polar Gln has the potential to influence the packing around this site and impact RNA interaction.

In the CTE domain, two variants, p.Val1090Met and p.Thr1101Met, have been studied. They are located in the same side of an α helix, although depending upon the cryo-EM structure, the helix N-terminus might be partly disorder [10]. This helix is close to the TR RNA, with Gly91 forming a hydrogen bond

with Arg1097 (Fig. 10B). Therefore, the substitution of Val1090 or Thr1101 by Met could potentially destabilize the interaction with the RNA.

The structural analysis revealed three mutations located near the interface of interaction with TPP1 (p.Val84Glu, p.Tyr772Cys) or POT1 (p.Pro65Thr, p.Val84Glu), two proteins of the shelterin complex. Val84 is situated in the central region of one α helix of TERT that interacts with TPP1 and POT1 through the C- and N-terminal regions, respectively (as shown in the structures of PDB code 7QXS, Fig. 10C). The p.Val84Glu mutant alters the hydrophobic face of the helix, which is tightly packed to another one, and could contribute to destabilize both the hydrophobic core around it and the interaction of TERT with TPP1 and/or POT1. Additionally, Tyr772 is located in a region involved in the interaction between TERT and TPP1 (structures of PDB code 7QXA, 7QXB and 7QXS), and participated in hydrogen bonds with residues Trp167 and Arg180 of this protein. Consequently, the p.Tyr772Cys variant might disrupt the protein–protein interface (Fig. 10D). Lastly, Pro65 is placed in a proline-rich loop close to a DNA region, which

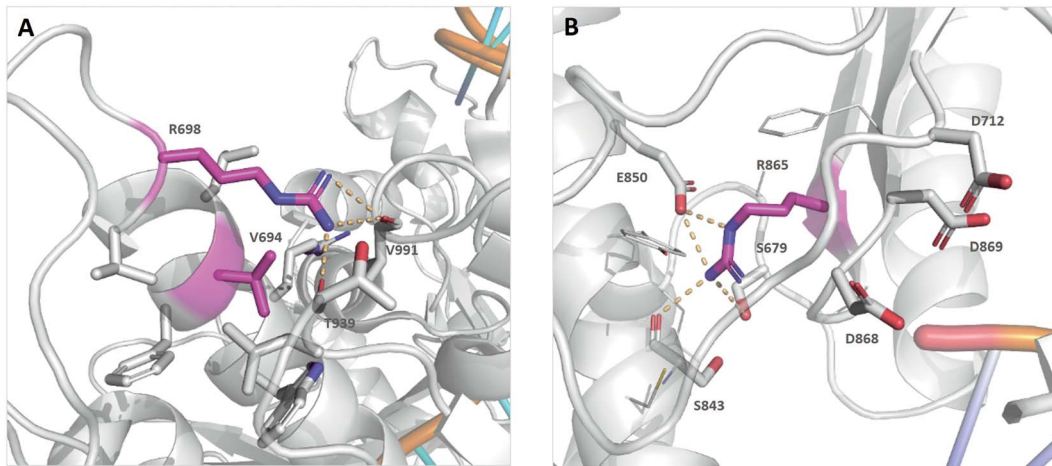


Figure 9. Structure of TERT reverse transcriptase (RT) domain regions containing the amino acid variants analyzed. Residues Val694, Arg698 and Arg865 (purple) from the RT domain (white), on the base of the structure of PDB code 7BG9. For clarity, only some of the amino acids side chains are depicted, and only polar hydrogens are shown. Polar contacts are indicated as yellow dotted lines. Panel A shows the position of residues Val694 and Arg698 while panel B shows the one of residue Arg865.

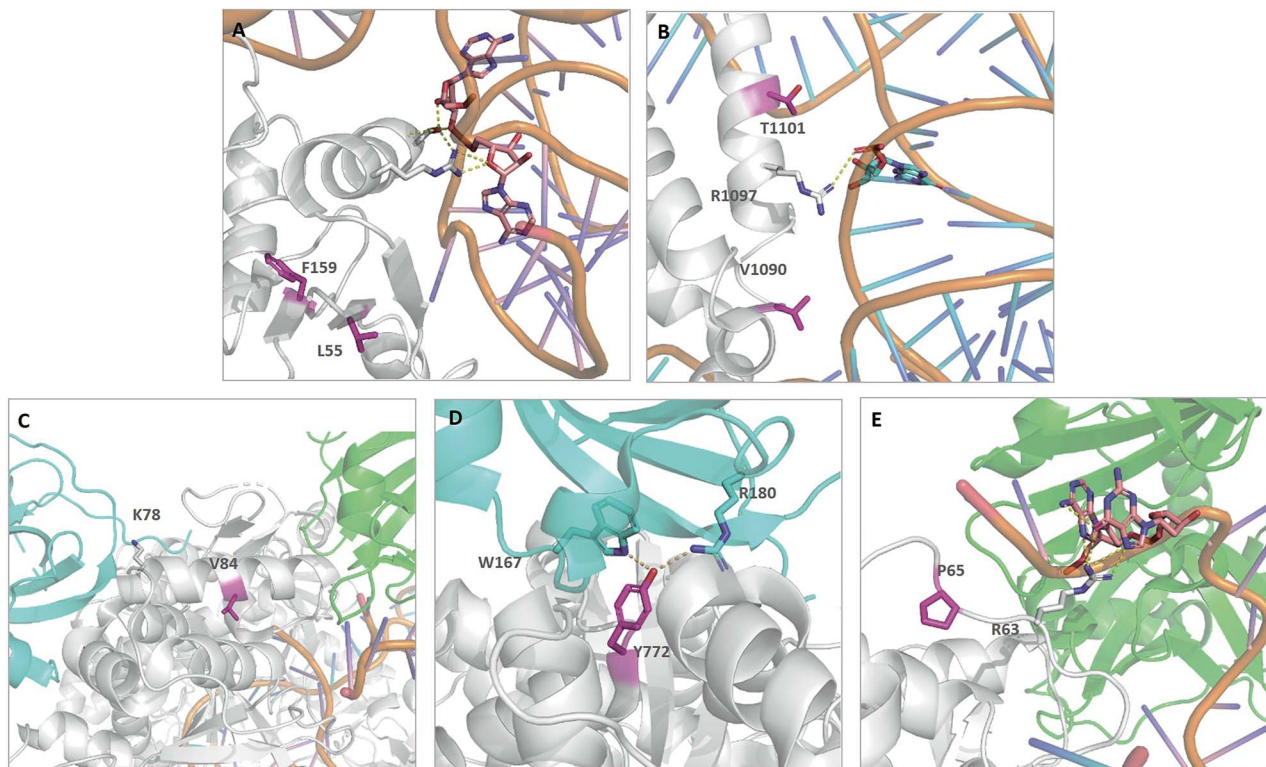


Figure 10. Structure of TERT regions involved in the interaction with the telomerase RNA, DNA and/or sheltering proteins containing amino acid variants analyzed in this article. Leu55 and Phe159 (purple) are located on a β -strand (panel A). Val1090 and Thr1101 (purple) in an α -helix close to the RNA region (orange, cyan, on the right) (panel B). Val84 (purple) is located in the middle of an α -helix, whose N-terminal domain is close to TPP1 (cyan on the left) and the C-terminus to POT1 (green on the right) (panel C). Residue Tyr772 (purple) is located in the interface of interaction with TPP1 (cyan on top) (panel D). Pro65 (purple) is located in a loop close to the DNA (orange) and POT1 (green at the bottom right) (panel E). Panels A and B correspond to the human telomerase structure of PDB code 7BG9; panels C, D and E to human telomerase of PDB code 7QXS. For clarity, only some of the amino acids side chains and polar hydrogens are shown. Polar contacts are depicted as yellow dotted lines.

is also interacting with POT1 (Fig. 10E). The p.Pro65Thr variant, in which proline has been replaced by a non-restricted amino acid, could lead to a change in the loop conformation and thus influence the interaction among TERT, DNA and POT1. However, the analysis of the available TERT structures in the PDB reveals that residue Ala202 is within a region that has not been possible to resolve.

Discussion

The functional effects of several variants found in TBD patients in the TERT and TERC genes have been studied in this article. Variants included several ones previously described in the literature as well as four TERT and one TERC variants found in Spanish TBD patients, four of them reported previously [41]. Functional

assays included the determination of *in vitro* telomerase activity using the TRAP assay but also extended to other functional alterations found in TBDs including the observed increase in oxidative stress and DNA damage. These additional functional alterations have not been previously analyzed for any of the reported *TERT* and *TERC* variants. The results obtained indicated that the expression of several variants increased oxidative stress, DNA guanine oxidation, DNA damage response and altered TRF2 telomere binding and cellular apoptosis (results summarized in [Supplementary Table S1](#)). Some of these functional alterations were observed in the 10 *TERT* missense variants and also in the 5 *TERC* variants. These assays were made in the WI-38 VA-13 cell line that presents minimal telomerase activity because telomeres are maintained by the Alternative Lengthening of Telomeres (ALT) mechanism. Although this cell line could be considered a non-physiological background because of this reason, it has been used for the analyses of telomerase activity of *TERT* and *TERC* variants in several previous studies (for example, [32, 42]). We have analyzed two *TERT* frame shift variants. One of them contains only 159 *TERT* residues and showed significant alterations in three of the functional parameters analyzed. The second frame shift variant analyzed contains 747 *TERT* residues and showed significant alterations in the same functional parameters, but to a lesser extent. These data could indicate that expression of the N-terminal domain of *TERT* might have a negative effect on different *TERT* functions that is larger when a shorter fragment is involved.

Several studies have described that *TERT* participates in different biological processes, beside telomere elongation, as already indicated in the Introduction section. Some of these activities might be related to the association of *TERT* with mitochondria that could be involved in the regulation of oxidative stress and apoptosis. Indeed, we have observed that under oxidative stress the expression of wild type *TERT/TERC* protects cells from apoptosis (Fig. 7). In addition, *TERT* associates with different transcription factors and could participate in gene expression regulation. *TERT* variants could alter some of these functions such as oxidative stress homeostasis. *TERT* variants could also alter telomere structure facilitating DNA oxidation and inducing DNA damage responses.

To get insights into the correlation between structural determinants and functional consequences of *TERT* variants, the studied mutants were mapped onto the cryo-EM structure of the complexes of human telomerase. Subsequently, potential alterations in the 3D structure surrounding each variant were analyzed and compared with the functional consequences identified in this study. Among the variants studied, those in which the amino acids were located in the reverse transcriptase domain of *TERT*, such as p.Val694Met, p.Arg698Trp and p.Arg865Cys were defective in enzymatic activity with minimal impact on the other functions analyzed, except for oxidative DNA damage at telomeres. The structural analyses indicated that substitution of Val694 and Arg698, both located in an RT domain helix (Fig. 9A), by Met and Trp, respectively, may disrupt protein packing, potentially affecting protein stability, and, consequently, enzymatic activity. On the other hand, the Arg865Cys variant's lack of enzymatic activity is likely due to a disruption of the catalytic center. This is because this residue is located on the same loop as the catalytic Asp712, and the conformation of this arginine is stabilized by a hydrogen bond network, which is not possible in the mutant (Fig. 9B). These observations are in agreement with a previous report that variant p.Val694Met severely decreases telomere elongation capacity of *TERT* [32, 43, 44]. Decreased catalytic activity and substantial decreased telomere elongation capacity were also reported for the

p.Arg865Hys variant, related to the p.Arg865Cys variant analyzed in this article [44, 45]. Similarly, the p.Arg698Gln variant affecting the same residue as p.Arg698Trp, has been described to produce severely reduced telomere elongation capacity [44]. It is noticeable that some of these variants, like p.Val694Met and p.Arg865Cys were associated with increased oxidative damage at telomeres and not to intracellular ROS levels. A similar result was obtained for the p.Val1090Met variant, that could affect *TERT/TERC* interaction and telomerase activity, as discussed later. We propose that this result could be explained if defective elongation could make telomeres more unprotected and sensitive to local oxidative damage and less dependent on ROS levels. This possibility would be in agreement with the observation that telomere DNA oxidation was more related to telomerase activity than to cellular oxidative stress in the variants analyzed, as shown in [Supplementary Fig. S5](#).

Several of the variants analyzed (p.Leu55Gln, p.Val1090Met, p.Thr1101Met) could alter the interaction between *TERT* and the TR RNA according to the structural analysis. Notably, variants p.Leu55Gln and p.Val1090Met, within the TEN and CTE domains, respectively, decreased telomerase activity while p.Thr1101Met in the CTE domain did not. The results presented in this article also indicate that some of these variants increased ROS production (Thr1101Met), guanine oxidation at telomeres (Val1090Met) or DNA damage response (Val1090Met). Interestingly, the CTE residues, located on the protein surface, are not involved in interactions within the protein core. The reduced telomerase activity observed in p.Leu55Gln and p.Val1090Met variants may be attributed to a disruption of *TERT*-RNA interface, as these residues are close to this interface, particularly Val1090 (Fig. 10A and B). The functional consequences of the p.Leu55Gln substitution on telomerase activity were previously described by Robart et al [42], that found that this change decreased primer extension and *TERT* interaction with TR. Besides, the p.Val1090Met variant has been described to produce a severe reduction in *TERT* elongation capacity [44]. In contrast, p.Thr1101Met, located close to the RNA interface (Fig. 10B), did not impact telomerase activity, although it increased ROS production. Despite involving the substitution of a polar residue by a hydrophobic one, the lack of impact on activity of this mutant might be explained by the fact that Thr1101 is not involved in polar interactions with either the protein or the RNA.

Some of the analyzed variants could interfere with the interaction of *TERT* and the shelterin complex proteins TPP1 (p.Val84Glu, p.Tyr772Cys) or POT1 (p.Pro65Thr, p.Val84Glu). In particular, the introduction of a negative charge due to the Val84Glu mutation likely disrupts the hydrophobic core, impacting the interaction with TPP1 and/or POT1 (Fig. 10C). It is worth to mention, that the mutation of another residue in the same helix, near the N-terminus, p.Lys78Glu, has been shown to maintain telomerase activity but to decrease stimulation by POT1-TPP1 and reduce telomere elongation capacity, which could be due to impaired telomere localization of *TERT* [46]. In agreement with these data, our results also show that the p.Val84Glu variant leads to decreased association of TRF2 with telomeres. However, decreased telomerase activity was also observed for the p.Val84Glu variant, which might be attributed to a disruption of *TERT* packing around this residue. On the other hand, although p.Tyr772Cys is located in the RT domain, this variant showed little alteration of the enzymatic activity, but the DNA damage response and cell apoptosis increased. Structural analysis showed that this tyrosine is at the interaction interface of *TERT* and TPP1 (Fig. 10D). Therefore, Tyr772Cys mutant prevents the formation of hydrogen bonds between this Tyr and TPP1 (Fig. 10D).

Interestingly, mutation of the nearby residues 771 (p.Pro771Leu) and 777 (p.Val777Met) led to a severe decrease in telomere elongation capacity [44]. This suggests that the latter residues are likely more relevant for TERT packing compared with Tyr772Cys. Finally, the functional analysis of Pro65Thr variant indicated that telomerase activity was not affected but there was an increase in DNA damage response at telomeres. Structural analyses showed that Pro65Thr mutation contribute to enhance the flexibility of the loop in which this Pro is located (Fig. 10E). This loop is in proximity to DNA and POT1, therefore, these interactions might be disrupted. The related p.Pro65Ala variant has been previously described as pathogenic [47]. Variants in the two residues involved in TPP1 interaction (p.Val84Glu, p.Tyr772Cys) increased apoptosis under oxidative stress conditions and were grouped together in the hierarchical analysis shown in Supplementary Fig. S5.

p.Ala202Thr mutant, situated in a region connecting the TEN and catalytic domains, is one of the variants that induced a larger number of phenotypic effects without affecting telomerase activity, ROS production, oxidative damage at telomeres, TRF2 recruitment, DDR at telomeres and apoptosis under oxidative stress. Although, in the analyzed structures, Ala202 residue and its surrounding sequence remains unresolved, it is tempting to suggest that p.Ala202Thr variant could alter the relative position of the TEN and catalytic domains. This variant has been described in two acquired aplastic anemia patients related to shortened telomeres [32].

The structure of the telomerase complex shows that the RNA component acts as a scaffold where the 5' domains (t/PK, CR4/CR5) interact with TERT while the 3' domain (ScaRNA domain) interact with the snoRNP proteins dyskerin, NOP10, NHP2 and RAP1. Among the variants analyzed, n.96_97delCT and n.98G > A are located in the t/PK domain, n.23G > C just upstream t/PK, and n.269G > A and n.325G > T in the CR4/CR5 domain. The variants n.23G > C, n.96_97delCT, n.98G > A and n.269G > A showed decreased telomerase activity, in agreement with their possible implication in TERT structure and activity. The n.269G > A also induced cell apoptosis. The n.96_97delCT and n.98G > A variants were previously analyzed by Robart *et al* [42], who found minimal primer extension activity for telomerase complexes containing these variants.

The n.23G > C variant is located in the P1A paired stem where it is complementary to another residue for which a pathogenic variant has been described, n.204C > G [48]. Stem P1A is predicted to be located between the two protein lobes and might be important for the structure of the telomerase complex. Expression of the n.23G > C variant increased ROS production, oxidation of telomeric DNA, DNA damage response and telomerase activity. Several other variants placed in this stem have been described in patients, such as n.202 T > G [49], n.204C > G [48] and n.20C > T [49] indicating its structural importance.

The 325 guanine, affected by the n.325G > T variant, is located in the 3' end of the P5 paired stem of the CR4/CR5 domain. Expression of this variant did not decrease *in vitro* telomerase activity but increased ROS production, DNA oxidation at telomeres and TRF2 recruitment. Variants n.322G > A [50], n.323C > T [51] and n.323C > G [52] have been also described in this RNA stem in myelodysplastic syndrome and pulmonary fibrosis patients.

The possible correlation between alterations in the different biological activities and the pathological manifestations of the patients carrying each variant is also of interest. Most variants from patients diagnosed of dyskeratosis congenita showed decreased *in vitro* telomerase activity (TERT p.Phe159CysfsTer32, p.Arg698Trp; TERC n.96_97delCT) [8, 41, 53], with the exception

of the variant p.Thr1101Met, that is described in this article. In contrast, most of the variants that presented high *in vitro* telomerase activity were identified in patients of pulmonary fibrosis (TERC n.325G > T) [47, 54] or aplastic anemia (TERT p.Pro65Thr, p.Ala202Thr, p.Tyr772Cys) [32, 55]. In addition, some of the variants identified in AA or IPF patients like TERT p.Val84Glu, identified in a patient presenting leukoplakia and thrombopenia [41], TERT p.Val1090Met (AA) [32], TERC n.23G > C (IPF) [41] or TERC n.325G > T (IPF) [54] produced alterations in several of the others parameters analyzed. The variants identified in DC patients produced increased DNA damage response (TERT p.Arg698Trp, TERC n.96_97delCT) or altered TRF2 association with telomeres (n.96_97delCT). This possible correlation between disease manifestations and the biological activity of the variants is only speculative and should be confirmed in a larger cohort of patients.

With respect to the variants that had not been analyzed previously, TERT p.Phe159CysfsTer32 is a frameshift deletion of two thymidine residues that affects telomerase activity, oxidative damage at telomere and ROS production. TERT p.Val84Glu alters all the parameters analyzed, TERC n.269G > A showed decreased *in vitro* telomerase activity and increased oxidative damage and DDR at telomeres while TERT p.Thr1101Met induced increased ROS production and TERT p.Pro65Thr higher DDR at telomeres. Therefore, we propose to consider these variants as pathogenic.

In conclusion, expression of TERT and TERC variants in an *in vitro* system using VA13 telomerase-deficient cells is useful to determine their *in vitro* telomerase activity but also to test their possible involvement in other biological activities such as the generation of oxidative stress, DNA damage response, apoptosis or the association of the shelterin complex with telomeres. Many of the variants analyzed showed decreased *in vitro* telomerase activity, as expected. In addition, some of them induced increased production of ROS, DNA oxidation at telomeres, altered localization of TRF2, increased DNA damage response or apoptosis. Many of the variants that affect these parameters correspond to residues located in TERT or TR domains involved in their interaction that are important for the structure of the telomerase complex. Some other TERT variants could alter the interaction between TERT and TPP1 or POT1 that are required for assembly of the telomerase complex and for regulation of its enzymatic activity. We speculate that weakening these interactions could increase the amount of TERT protein not associated to telomeres and its extra-telomeric activities inducing oxidative stress and/or oxidation of telomeric DNA that would result in increased DNA damage, genetic instability and apoptosis. The observed decreased TRF2 association to telomeres induced by the expression of some variants could also contribute to telomere instability with similar effects in DNA damage, oxidative stress and apoptosis.

Materials and methods

Plasmids, cloning and site-directed mutagenesis

Point mutations were generated from the retroviral dual expression vector pBABE-TERT/TERC described by Wong and Collins [56], on loan from Dr Kathleen Collins (University of California, Berkeley, CA, USA). This vector contains the TERT (NM_001193376.1) and TERC (NR_001566.1) WT genes preceded by independent constitutive promoters. Mutations in TERT and TERC described in patients with telomeropathies were generated following the *in vitro* directed mutagenesis protocol of Zheng [57]. Plasmid DNA from the retroviral vectors was extracted with the Plasmid Maxi

in blocking solution (TRF2: ab13579; 53BP1: ab36823 Abcam). Cells were washed three times with PBS-Tween 20 (0.1%) and incubated with secondary antibody diluted in blocking solution for 1 h at room temperature in the dark. Cells were washed three times with PBS-Tween 20 (0.1%), fixed again with 3.7% PFA, dehydrated with graded ethanol (70%, 90%, 100%) and air dried. TelC-Alexa488 (F-1004) or TelC-Cy3(F-1002) telomere probes (CCCTAA repeats; PNABIO, Thousand Oaks, CA, USA) were diluted in hybridization buffer and incubated with cells at 80°C for 5 min followed by incubation at room temperature for 60 min. After hybridization, cells were washed with PNA wash A (70% formamide, 10 mmol/L Tris-Cl pH 7.5) twice followed by three washes with PNA wash B (50 mmol/L Tris-Cl pH 7.5, 150 mmol/L NaCl, 0.8% Tween 20). DAPI was added to PNA wash B buffer in the second wash to counterstain DNA. Coverslips were dehydrated with graded ethanol, air dried, and mounted with prolong gold (P36934; Life Technologies). Image acquisition was performed with a Nikon Eclipse 90i microscope and a 40x lens. Image treatment was done with ImageJ software. Foci and co-localization were calculated with Cell Profiler. TRF2-TelC and 53BP1-TelC overlapping indexes were quantified and normalized to pBABE-WT TERT/TERC in five different microscopy fields, analyzing an average of 200 cells/experiment.

Immunofluorescence analysis (γ H2AX)

Cells were seeded on coverslips in 24-well plates (15 000–20 000 cells per well) for observation with confocal microscopy. Cells were fixed with 3.7% PFA for 10 min. Permeabilization was performed by incubation with 0.5% Triton X-100 in PBS for 15 min. Cells were washed with PBS twice and blocked for 1 h at room temperature with blocking solution (3% BSA complemented with 0.1% Tween 20 in PBS). Cells were incubated overnight with the primary antibody in blocking solution (γ H2AX: 05-636; Millipore). Cells were washed three times with PBS-Tween 20 (0.1%) and incubated with secondary antibody diluted in blocking solution for 1 h at room temperature in the dark. Cells were washed three times with PBS-Tween 20 (0.1%) and nuclei were stained with 0.5 μ g/ml DAPI. Coverslips were washed three times (10 min in PBS each time) and mounted. Image acquisition was performed with a Zeiss Axio Observer/Cell Observer. Coverslips were scanned and 25 fields were acquired at 20x (average of 12 000 cells/experiment). Nuclear fluorescence signal of γ H2AX was determined using Cell Profiler.

Statistical analyses

The statistical method and details about the data are described in the caption for each of the figures containing any statistics. In brief, the mean was used to measure the main tendency of the data, and the standard error of the mean was used for dispersion measurement. All statistical analysis was performed using PRISM software (GraphPad Software, Inc., La Jolla, CA, USA). The differences between the mean values of each group were compared using a two-tailed unpaired t-test (* $P < 0.05$; ** $P < 0.01$; *** $P < 0.001$).

Supplementary data

Supplementary data is available at HMG Journal online.

Conflict of Interest statement: The authors declare no conflict of interest.

Funding

This work was supported by Fondo de Investigaciones Sanitarias, Instituto de Salud Carlos III, Spain, co-funded by European Regional Development (FEDER) funds [grant number PI20-00335] and Consejo Superior de Investigaciones Científicas, Spain [grant PIE-202180E073]. BF-V was funded by a contract from Comunidad Autónoma de Madrid and the Fondo Social Europeo as part of the iniciativa de Empleo Juvenil (YEI), Spain. CB-B was funded by a postdoctoral contract from the Fundación Científica Asociación Española Contra el Cáncer (AECC) [POSTD20042BENI].

References

- Chakravarti D, LaBella KA, DePinho RA. Telomeres: history, health, and hallmarks of aging. *Cell* 2021;**184**:306–22.
- Kam MLW, Nguyen TTT, Ngeow JYY. Telomere biology disorders. *NPJ Genom Med* 2021;**6**:36.
- Armanios M. The role of telomeres in human disease. *Annu Rev Genomics Hum Genet* 2022;**23**:363–81.
- Levy MZ, Allsopp RC, Fletcher AB. et al. Telomere end-replication problem and cell aging. *J Mol Biol* 1992;**225**:951–60.
- Lopez-Otin C, Blasco MA, Partridge L. et al. The hallmarks of aging. *Cell* 2013;**153**:1194–217.
- Bertuch AA. The molecular genetics of the telomere biology disorders. *RNA Biol* 2016;**13**:696–706.
- Grill S, Nandakumar J. Molecular mechanisms of telomere biology disorders. *J Biol Chem* 2021;**296**:100064.
- Vulliamy T, Marrone A, Szydlo R. et al. Disease anticipation is associated with progressive telomere shortening in families with dyskeratosis congenita due to mutations in TERC. *Nat Genet* 2004;**36**:447–9.
- Nguyen THD, Tam J, Wu RA. et al. Cryo-EM structure of substrate-bound human telomerase holoenzyme. *Nature* 2018;**557**:190–5.
- He Y, Wang Y, Liu B. et al. Structures of telomerase at several steps of telomere repeat synthesis. *Nature* 2021;**593**:454–9.
- Wu RA, Upton HE, Vogan JM. et al. Telomerase mechanism of telomere synthesis. *Annu Rev Biochem* 2017;**86**:439–60.
- Li L, Ye K. Crystal structure of an H/ACA box ribonucleoprotein particle. *Nature* 2006;**443**:302–7.
- Nandakumar J, Bell CF, Weidenfeld I. et al. The TEL patch of telomere protein TPP1 mediates telomerase recruitment and processivity. *Nature* 2012;**492**:285–9.
- Nandakumar J, Cech TR. Finding the end: recruitment of telomerase to telomeres. *Nat Rev Mol Cell Biol* 2013;**14**:69–82.
- Frescas D, de Lange T. Binding of TPP1 protein to TIN2 protein is required for POT1a,b protein-mediated telomere protection. *J Biol Chem* 2014;**289**:24180–7.
- Bisht K, Smith EM, Tesmer VM. et al. Structural and functional consequences of a disease mutation in the telomere protein TPP1. *Proc Natl Acad Sci USA* 2016;**113**:13021–6.
- Liu N, Ding D, Hao W. et al. hTERT promotes tumor angiogenesis by activating VEGF via interactions with the Sp1 transcription factor. *Nucleic Acids Res* 2016;**44**:8693–703.
- Wu L, Wang S, Tang B. et al. Human telomerase reverse transcriptase (hTERT) synergistic with Sp1 upregulate Gli1 expression and increase gastric cancer invasion and metastasis. *J Mol Histol* 2021;**52**:1165–75.
- Park JI, Venteicher AS, Hong JY. et al. Telomerase modulates Wnt signalling by association with target gene chromatin. *Nature* 2009;**460**:66–72.
- Santos JH, Meyer JN, Van Houten B. Mitochondrial localization of telomerase as a determinant for hydrogen

- peroxide-induced mitochondrial DNA damage and apoptosis. *Hum Mol Genet* 2006;**15**:1757–68.
21. Indran IR, Hande MP, Pervaiz S. hTERT overexpression alleviates intracellular ROS production, improves mitochondrial function, and inhibits ROS-mediated apoptosis in cancer cells. *Cancer Res* 2011;**71**:266–76.
 22. Sahin E, Colla S, Liesa M. et al. Telomere dysfunction induces metabolic and mitochondrial compromise. *Nature* 2011;**470**:359–65.
 23. Podlevsky JD, Bley CJ, Omana RV. et al. The telomerase database. *Nucleic Acids Res* 2008;**36**:D339–43.
 24. Kermasson L, Churikov D, Awad A. et al. Inherited human Apollo deficiency causes severe bone marrow failure and developmental defects. *Blood* 2022;**139**:2427–40.
 25. Armanios M, Blackburn EH. The telomere syndromes. *Nat Rev Genet* 2012;**13**:693–704.
 26. Sholes SL, Karimian K, Gershman A. et al. Chromosome-specific telomere lengths and the minimal functional telomere revealed by nanopore sequencing. *Genome Res* 2022;**32**:616–28.
 27. Lee HW, Blasco MA, Gottlieb GJ. et al. Essential role of mouse telomerase in highly proliferative organs. *Nature* 1998;**392**:569–74.
 28. Alder JK, Barkauskas CE, Limjunyawong N. et al. Telomere dysfunction causes alveolar stem cell failure. *Proc Natl Acad Sci USA* 2015;**112**:5099–104.
 29. Gu BW, Fan JM, Bessler M. et al. Accelerated hematopoietic stem cell aging in a mouse model of dyskeratosis congenita responds to antioxidant treatment. *Aging Cell* 2011;**10**:338–48.
 30. Manguan-Garcia C, Pintado-Berninches L, Carrillo J. et al. Expression of the genetic suppressor element 24.2 (GSE24.2) decreases DNA damage and oxidative stress in X-linked dyskeratosis congenita cells. *PLoS One* 2014;**9**:e101424.
 31. Armanios M, Chen JL, Chang YP. et al. Haploinsufficiency of telomerase reverse transcriptase leads to anticipation in autosomal dominant dyskeratosis congenita. *Proc Natl Acad Sci USA* 2005;**102**:15960–4.
 32. Yamaguchi H, Calado RT, Ly H. et al. Mutations in TERT, the gene for telomerase reverse transcriptase, in aplastic anemia. *N Engl J Med* 2005;**352**:1413–24.
 33. Gramatges MM, Qi X, Sasa GS. et al. A homozygous telomerase T-motif variant resulting in markedly reduced repeat addition processivity in siblings with Hoyeraal Hreidarsson syndrome. *Blood* 2013;**121**:3586–93.
 34. Singhapol C, Pal D, Czapiewski R. et al. Mitochondrial telomerase protects cancer cells from nuclear DNA damage and apoptosis. *PLoS One* 2013;**8**:e52989.
 35. Michel M, Benitez-Buelga C, Calvo PA. et al. Small-molecule activation of OGG1 increases oxidative DNA damage repair by gaining a new function. *Science* 2022;**376**:1471–6.
 36. Coluzzi E, Leone S, Sgura A. Oxidative stress induces telomere dysfunction and senescence by replication fork arrest. *Cells* 2019;**8**:19.
 37. Fouquerel E, Lormand J, Bose A. et al. Oxidative guanine base damage regulates human telomerase activity. *Nat Struct Mol Biol* 2016;**23**:1092–100.
 38. Qian W, Kumar N, Roginskaya V. et al. Chemoptogenetic damage to mitochondria causes rapid telomere dysfunction. *Proc Natl Acad Sci USA* 2019;**116**:18435–44.
 39. Ghanim GE, Fountain AJ, van Roon AM. et al. Structure of human telomerase holoenzyme with bound telomeric DNA. *Nature* 2021;**593**:449–53.
 40. Sekne Z, Ghanim GE, van Roon AM. et al. Structural basis of human telomerase recruitment by TPP1-POT1. *Science* 2022;**375**:1173–6.
 41. Arias-Salgado EG, Galvez E, Planas-Cerezales L. et al. Genetic analyses of aplastic anemia and idiopathic pulmonary fibrosis patients with short telomeres, possible implication of DNA-repair genes. *Orphanet J Rare Dis* 2019;**14**:82.
 42. Robart AR, Collins K. Investigation of human telomerase holoenzyme assembly, activity, and processivity using disease-linked subunit variants. *J Biol Chem* 2010;**285**:4375–86.
 43. Zaug AJ, Crary SM, Jesse Fioravanti M. et al. Many disease-associated variants of hTERT retain high telomerase enzymatic activity. *Nucleic Acids Res* 2013;**41**:8969–78.
 44. Reilly CR, Myllymaki M, Redd R. et al. The clinical and functional effects of TERT variants in myelodysplastic syndrome. *Blood* 2021;**138**:898–911.
 45. Tsakiri KD, Cronkhite JT, Kuan PJ. et al. Adult-onset pulmonary fibrosis caused by mutations in telomerase. *Proc Natl Acad Sci USA* 2007;**104**:7552–7.
 46. Schmidt JC, Dalby AB, Cech TR. Identification of human TERT elements necessary for telomerase recruitment to telomeres. *Elife* 2014;**3**:e03563.
 47. Calado RT, Regal JA, Hills M. et al. Constitutional hypomorphic telomerase mutations in patients with acute myeloid leukemia. *Proc Natl Acad Sci USA* 2009;**106**:1187–92.
 48. Fogarty PF, Yamaguchi H, Wiestner A. et al. Late presentation of dyskeratosis congenita as apparently acquired aplastic anaemia due to mutations in telomerase RNA. *Lancet* 2003;**362**:1628–30.
 49. Collopy LC, Walne AJ, Cardoso S. et al. Triallelic and epigenetic-like inheritance in human disorders of telomerase. *Blood* 2015;**126**:176–84.
 50. Yamaguchi H, Baerlocher GM, Lansdorp PM. et al. Mutations of the human telomerase RNA gene (TERC) in aplastic anemia and myelodysplastic syndrome. *Blood* 2003;**102**:916–8.
 51. Junko T, Ly H, Yamaguchi H. et al. Identification and functional characterization of novel telomerase variant alleles in Japanese patients with bone-marrow failure syndromes. *Blood Cells Mol Dis* 2008;**40**:185–91.
 52. Justet A, Klay D, Porcher R. et al. Safety and efficacy of pirfenidone and nintedanib in patients with idiopathic pulmonary fibrosis and carrying a telomere-related gene mutation. *Eur Respir J* 2021;**57**:2003198.
 53. Carrillo J, Martinez P, Solera J. et al. High resolution melting analysis for the identification of novel mutations in DKC1 and TERT genes in patients with dyskeratosis congenita. *Blood Cells Mol Dis* 2012;**49**:140–6.
 54. Alder JK, Chen JJ, Lancaster L. et al. Short telomeres are a risk factor for idiopathic pulmonary fibrosis. *Proc Natl Acad Sci USA* 2008;**105**:13051–6.
 55. Vulliamy TJ, Walne A, Baskaradas A. et al. Mutations in the reverse transcriptase component of telomerase (TERT) in patients with bone marrow failure. *Blood Cells Mol Dis* 2005;**34**:257–63.
 56. Wong JM, Collins K. Telomerase RNA level limits telomere maintenance in X-linked dyskeratosis congenita. *Genes Dev* 2006;**20**:2848–58.
 57. Zheng L, Baumann U, Reymond JL. An efficient one-step site-directed and site-saturation mutagenesis protocol. *Nucleic Acids Res* 2004;**32**:e115.
 58. Machado-Pinilla R, Sanchez-Perez I, Murguía JR. et al. A dyskerin motif reactivates telomerase activity in X-linked dyskeratosis congenita and in telomerase-deficient human cells. *Blood* 2008;**111**:2606–14.
 59. Armanios MY, Chen JJ, Cogan JD. et al. Telomerase mutations in families with idiopathic pulmonary fibrosis. *N Engl J Med* 2007;**356**:1317–26.